Comparison of the linear and non-linear SGS models in simulating the internal flow in a centrifugal pump impeller

Huang Xianbei, Liu Zhuqing, Yang Wei, Li Yaojun, Tang Xuelin

ISROMAC 2016

International Symposium on Transport Phenomena and Dynamics of Rotating Machinery

Hawaii, Honolulu

April 10-15, 2016

Abstract

In this paper, the performances of linear and non-linear SGS models are compared by simulating a centrifugal pump impeller at both design load and quarter load. The mesh convergence is studied to choose the mesh with 2.05 million. At design load, the flow behaves well in both channels and the two models perform similarly. While at quarter load, the "two-channel" flow pattern occurs. Although this phenomenon is detected by both models, the peak value of the velocity profile moves towards the pressure side, showing opposite tendency to PIV. Comparing the two models under this condition, DNM shows significant priority over DSM due to the improved relation between the SGS stress, the shear-stress and the vorticity.

Keywords

SGS — centrifugal pump — non-linear

Beijing Engineering Research Center of Safety and Energy Saving Technology for Water Supply Network System, College of Water Resources and Civil Engineering, China Agricultural University, Beijing, China

***Corresponding author**: lzq@cau.edu. cn

INTRODUCTION

Large eddy simulation (LES) has been developed for several decades since the pioneer works of Smagorinsky [1] and Deardorff [2]. The Smagorinsky Model (SM), including the dynamic version (DSM), adopts a linear relationship between the SGS stress tensor and the strain-rate tensor. According to the results from Tao et al [3] and Horiuti [4], the linear relationship adopted by SM is actually not hold. Kosovic [5] proposed a polynomial (non-linear) relation of SGS stress which depended on both the strain rate and the vorticity. Wang et al [6] extended the model by applying the dynamic procedure proposed by Germano [7], named DNM here after.

As a typical turbo-machine, centrifugal pump plays an important role in industry. Due to the superior accuracy, LES attracts more concentrations in the field of centrifugal pump's research and design. In most commercial CFD codes, only linear SGS models are included. However, the results from linear models are not so satisfying, especially at off-design conditions [8]. It is necessary to test the performance of the non-linear SGS model.

As the implementation of new model into these codes is relatively fussy, the open-source code OpenFOAM [9] is used in this paper. For comparison, the linear model DSM and the non-linear model DNM are used in simulating the flow in a centrifugal pump impeller. The calculation results are compared with the PIV results by Pedersen et al [8].

1. FORMULATIONS

1.1 Filtered Navier-Stokes equations

In LES, a low-pass filter (in frequency) is applied to the Navier-Stokes equations to get the following formulations (in Cartesian coordinate):

$$\frac{\partial(\rho\bar{u}_i)}{\partial x_i}=0 \tag{1}$$

$$\frac{\partial\bar{u}_i}{\partial t}+\frac{\partial}{\partial x_j}\left(\bar{u}_i\bar{u}_j\right)=-\frac{1}{\rho}\frac{\partial\bar{p}}{\partial x_i}+\frac{\partial}{\partial x_j}\left[\nu\left(\frac{\partial\bar{u}_i}{\partial x_j}+\frac{\partial\bar{u}_j}{\partial x_i}\right)\right]+\frac{\partial\tau_{ij}}{\partial x_j}+S_i \tag{2}$$

where, the variables with an over bar represent the filtered quantities, u represents the velocity, p

is the pressure, ν is the kinetic viscosity, S_i is the source term and τ_{ij} is the SGS stress , which is defined as

$$\tau_{ij} = \overline{u}_i \overline{u}_j - \overline{u_i u_j} \tag{3}$$

1.2 SGS models

1.2.1 DSM

DSM is a linear eddy-viscosity model. The SGS stress can be expressed as:

$$\tau_{ij}^{\ d} = -2\nu_r \overline{S}_{ij} \tag{4}$$

where $\overline{S}_{ij}$ is the rate-of-strain tensor, $\tau_{ij}^{\ d}$ is the deviatoric part of the SGS stress tensor to be modeled because $\overline{S}_{ij}$ is zero-trace. ν_r is the eddy viscosity with

$$\nu_r = c_s \overline{\Delta}^2 \left|\overline{S}\right| \tag{5}$$

where $\overline{\Delta}$ is the filter width and $\left|\overline{S}\right| = (2\overline{S}_{ij}\overline{S}_{ij})^{1/2}$ is the characteristic filtered rate of strain. The final form of the Smagorinsky model is obtained as:

$$\tau_{ij}^{\ d} = -2c_s \overline{\Delta}^2 \left|\overline{S}\right| \overline{S}_{ij} \tag{6}$$

In order to dynamically calculate c_s, Germano [7] proposed to apply a second filter called the test filter to the SGS stress:

$$\begin{aligned} T_{ij} &= (\overline{u}_i \overline{u}_j - \overline{u_i u_j}), \\ L_{ij} &= T_{ij} - \tilde{\tau}_{ij} \end{aligned} \tag{7}$$

here, '~' denotes test-filtering operation, T_{ij} is the stress at a test filter scale($\overline{\Delta} = 2\overline{\Delta}$).Similarly to equation (6)

$$T_{ij}^{\ d} = -2c_s \overline{\Delta}^2 \left|\overline{S}\right| \overline{S}_{ij} \tag{8}$$

where $T_{ij}^{\ d}$ is the deviatoric part of T_{ij} . Combining equations (6) and (8):

$$\begin{aligned} T_{ij}^{\ d} - \overline{\tau}_{ij}^{d} &= 2c_s \overline{\Delta}^2 \left|\overline{S}\right| \overline{S}_{ij} - \\ 2c_s \overline{\Delta}^2 \left|\overline{S}\right| \overline{S}_{ij} &= c_s M_{ij} \end{aligned} \tag{9}$$

Using equation (9) to provide an approximation to L_{ij}^d:

$$L_{ij}^d = c_s M_{ij} \tag{10}$$

Least squares minimization of the error is suggested to be used by Lilly [10] to calculate the value of c_s:

$$c_s = \frac{M_{ij} L_{ij}}{M_{kl} M_{kl}} \tag{11}$$

It is well known that DSM suffers from numerical instability due to the large oscillation of the model coefficient. In this paper, the eddy viscosity is bounded as:

$$\nu_r = \max(\nu_r, -\nu) \tag{12}$$

which means that the backscatter can't be larger than the viscous dissipation.

1.2.2 DNM

Kosovic [5] proposed a non-linear model which is a simplification of the model investigated by Lund and Novikov [11]. The model can be written as:

$$\begin{aligned} \tau_{ij}^{d} &= c_s \overline{\Delta}^2 \left|\overline{S}\right| \overline{S}_{ij} + c_1 \overline{\Delta}^2 (\overline{S}_{ik} \overline{\Omega}_{kj} \\ &- \overline{\Omega}_{ik} \overline{S}_{kj}) + c_2 \overline{\Delta}^2 (\overline{S}_{ik} \overline{S}_{kj} - \frac{1}{3} \overline{S}_{mn} \overline{S}_{nm} \delta_{ij}) \end{aligned} \tag{13}$$

here $\overline{\Omega}_{ij}$ is the vorticity, the condition $\overline{\Delta} = 2\overline{\Delta}$ is applied. Wang et al [6] propose to apply Germano's method [7] to the SGS stress:

$$T_{ij}^{d} = 4c_s\overline{\Delta}^2\left|\overline{S}\right|\tilde{\overline{S}}_{ij} + 4c_1\overline{\Delta}^2(\tilde{\overline{S}}_{ik}\overline{\Omega}_{kj} - \overline{\Omega}_{ik}\tilde{\overline{S}}_{kj}) + 4c_2\overline{\Delta}^2(\tilde{\overline{S}}_{ik}\tilde{\overline{S}}_{kj} - \frac{1}{3}\tilde{\overline{S}}_{mn}\tilde{\overline{S}}_{nm}\delta_{ij}) \quad (14)$$

$$\tilde{\tau}_{ij}^{d} = c_s\overline{\Delta}^2\left|\overline{S}\right|\overline{S}_{ij} + c_1\overline{\Delta}^2(\overline{S}_{ik}\overline{\Omega}_{kj} - \overline{\Omega}_{ik}\overline{S}_{kj}) + c_2\overline{\Delta}^2(\overline{S}_{ik}\overline{S}_{kj} - \frac{1}{3}\overline{S}_{mn}\overline{S}_{nm}\delta_{ij}) \quad (15)$$

Use Lily's least squares [10] to finally determine the three model coefficients:

$$\begin{bmatrix} M_{ij}M_{ij} & M_{ij}N_{ij} & M_{ij}P_{ij} \\ N_{ij}M_{ij} & N_{ij}N_{ij} & N_{ij}P_{ij} \\ P_{ij}M_{ij} & P_{ij}N_{ij} & P_{ij}P_{ij} \end{bmatrix}\begin{bmatrix} c_s \\ c_1 \\ c_2 \end{bmatrix} = \begin{bmatrix} M_{ij}L_{ij}^{d} \\ N_{ij}L_{ij}^{d} \\ P_{ij}L_{ij}^{d} \end{bmatrix} \quad (16)$$

where

$$M_{ij} = 4\overline{\Delta}^2\left|\overline{S}\right|\tilde{\overline{S}}_{ij} - \overline{\Delta}^2\left|\overline{S}\right|\overline{S}_{ij} \quad (17)$$

$$N_{ij} = 4\overline{\Delta}^2(\overline{S}_{ik}\overline{\Omega}_{kj} - \overline{\Omega}_{ik}\overline{S}_{kj}) - \overline{\Delta}^2(\overline{S}_{ik}\overline{\Omega}_{kj} - \overline{\Omega}_{ik}\overline{S}_{kj}) \quad (18)$$

$$P_{ij} = 4\overline{\Delta}^2(\tilde{\overline{S}}_{ik}\tilde{\overline{S}}_{kj} - \frac{1}{3}\tilde{\overline{S}}_{mn}\tilde{\overline{S}}_{nm}\delta_{ij}) - \overline{\Delta}^2(\overline{S}_{ik}\overline{S}_{kj} - \frac{1}{3}\overline{S}_{mn}\overline{S}_{nm}\delta_{ij}) \quad (19)$$

2. RESULTS AND DISCUSSION

2.1 Grid convergence analysis

The impeller under investigated is a shrouded, low specific–speed (dimensionless specific-speed $N_s = 0.5$) multistage pump as shown in Figure 1. Pedersen's results have shown that stalls will appear in every two adjacent channels at quarter-load [8]. Therefore, in order to reduce the computational resource, two channels are used for calculation.

In this paper, we use the procedure proposed by Celik et al [12] to examine whether the grid has been in the asymptotic range. To resolve the near-wall characteristics, the y^+ is set to locate in the viscous sub-layer at all the walls including blade, hub and shroud. Three grids are generated, with the element number equal to 4.17×10^5, 9.13×10^5 and 2.05×10^6 respectively.

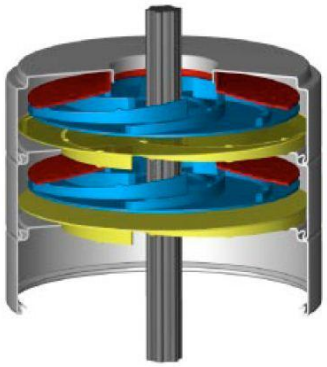

Figure 1. Two stages of the investigated centrifugal pump

The velocity inlet condition is applied at inlet. At the impeller outlet, a static pressure is applied. The whole domain is calculated in the rotating frame. Rotational periodic conditions are applied to the two sides of the domain. All the walls are fully resolved without near wall treatment.

As for the numerical schemes, 'Gauss linear' scheme (second order) is chosen for the gradient term, and the second order upwind scheme named 'Gauss linearUpwind' is used for the divergence term. The time scheme is the second order implicit 'backward' scheme. The time-step size is chosen to ensure an average Courant number smaller than 0.5. The averaging process is turned on when the flow field is statistically stable, and another 5000 time-steps are taken to calculate the time-averaged properties. The radial (U_r) and (U_t) tangential relative velocities on the mid-height plane ($z/b_2 = 0.5$) at radial positions of $0.5R_2$ and $0.9R_2$ are used for the grid convergence study, where z is the blade height direction from hub to shroud, b_2 is the outlet width and R_2 is the impeller outlet radius. Figure 2 shows the extrapolated velocity (the velocity

obtained by Richardson extrapolation) distributions and the results of the finest mesh at design load.

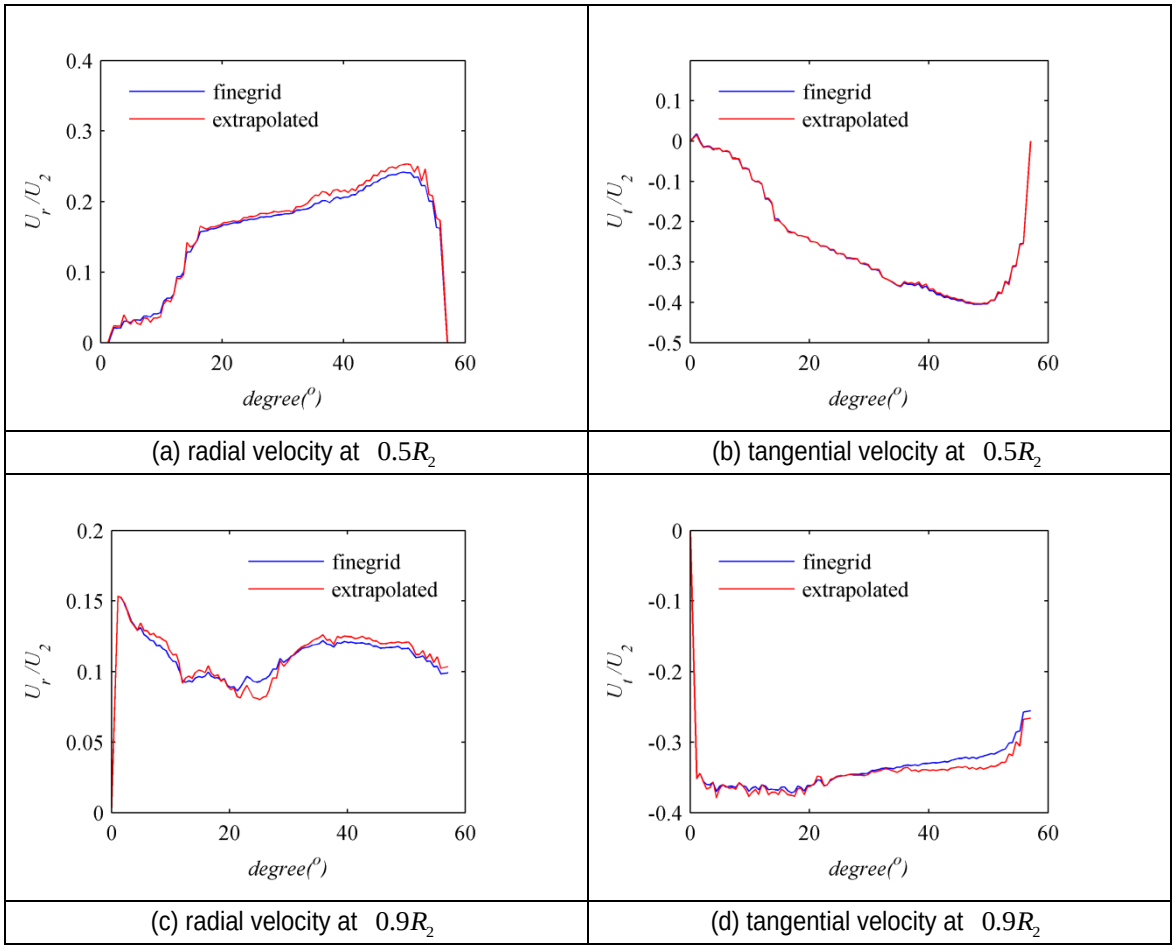

Figure 2. Radial and tangential velocity profiles

In addition, as the flow fields in the two channels are almost the same, only one channel is plotted. The velocities are nondimensionalized by the impeller outlet velocity U_2. As can be seen from Figure 2, the extrapolated velocities are close to these of the fine grid, which is a good indication that convergence been reached. In the following calculations, the mesh with 2.05×10^6 elements is used.

2.2 Comparison of two models

2.2.1 design load

Figure 3 shows the comparison of time-averaged radial and tangential relative velocities on the mid-height plane at radial positions of $0.5R_2$ and $0.9R_2$ at design load. As can be seen, the velocity profiles maintain the same trend, with some deviations between the two channels. Significant slopes of U_r and U_t curves can be found at $0.5R_2$. It's mainly caused by the Coriolis force in rotating parts. At a moderate radius ($0.5R_2$), the effect of centrifugal force is not so strong comparing with the Coriolis, therefore, the flow is driven by this force and results in a slope of the velocity as can be seen in Figure 3(a), (b). While at $0.9R_2$, the

centrifugal force becomes the dominant effect, thus the flow is much more uniform.

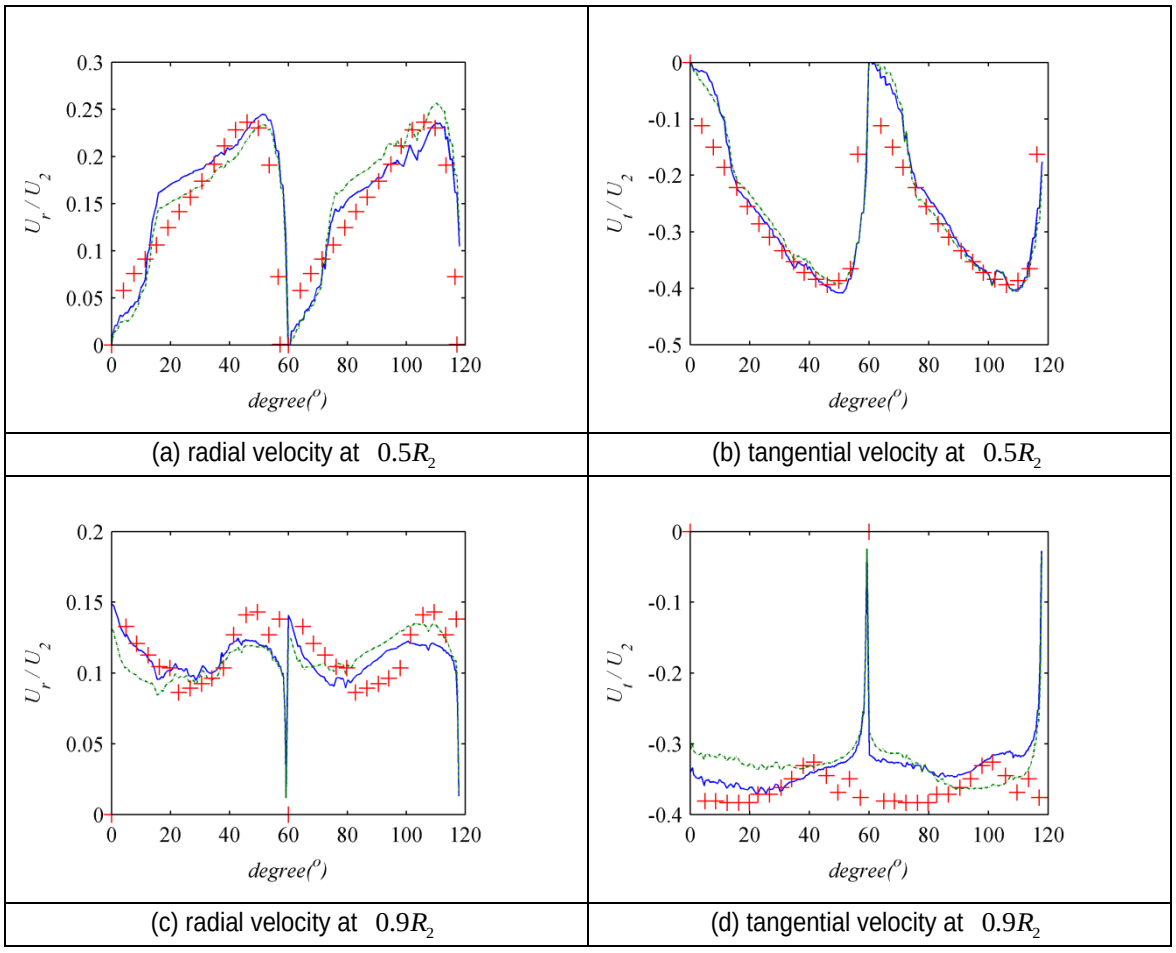

(a) radial velocity at $0.5R_2$ (b) tangential velocity at $0.5R_2$

(c) radial velocity at $0.9R_2$ (d) tangential velocity at $0.9R_2$

Figure 3. Comparison of Radial and tangential velocity profiles at design load(—:DSM, --:DNM, +:PIV results)

2.2.2 quarter load

At quarter load, clear rotating stall is detected in one of the two channels, showing a “two-channel” flow pattern. Flow in channel B is dominated by the rotating effect and behaves well as in design load, while channel A is influenced by the secondary flow and generates a stationary stall. The rotating stall in channel A near the outlet of the blade from the result of DSM is shown in Figure 4, for clear illustration, every 40 vectors are shown. The green lines imply the blade’s pressure and suction sides.

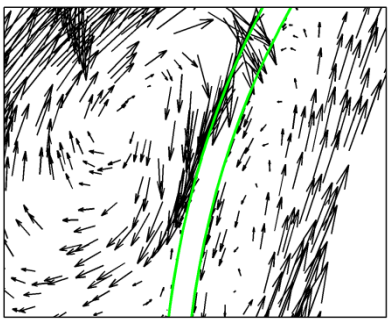

Figure 4. Time-averaged stall by DSM at pressure side near the outlet in channel A (left)

According to Pedersen et al [8], this kind of stationary stall is related to the even number of the impeller passages which enables a stable equilibrium between the forces acting on the stall. In fact, Zhou [13] studied centrifugal pump impellers with different number of blades and found that only impeller with even blades can maintain stationary stalls at off-design load.

As the flow patterns in the two channels are different, the velocity profiles are inevitably affected. Figure 5 shows the comparison of time-averaged radial and tangential relative velocities on the mid-height plane at radial positions of $0.5R_2$ and $0.9R_2$ at design load.

As can be seen, the velocity profiles of the two channels are different. The tendency of the predicted profiles of channel A agree with the PIV data, while for the profiles of channel B, the simulations show significant difference from PIV with the peak position moves towards the pressure side (at position 60°). Pedersen et al [8] attribute it to the prerotation at inlet caused by the rotational effect and the leakage flow in the experiment, which is disregarded in the simulation. While they didn't explain why channel A is not affected. In fact, when the "two-channel" flow pattern occurs, the turbulence intensity in channel A would be much larger than that in channel B, therefore, the prerotation at inlet can easily affect the flow field in channel B while hardly to change that in channel A. Comparing the two models, it's obvious that DNM performs much better than DSM, especially in channel A. This is due to the much closer relation between the SGS tensor and the vorticity and shear-strain in DNM comparing to the linear relationship in DSM. The advantage of the non-linear model is better reflected under high-turbulence level condition as at quarter-load condition.

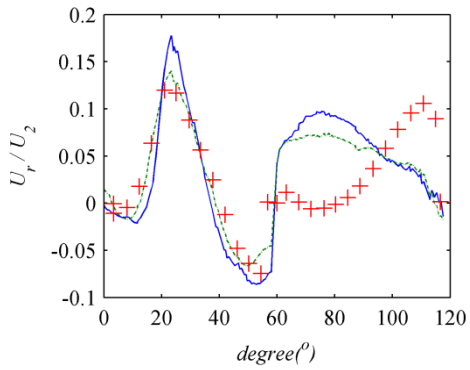

(a) radial velocity at $0.5R_2$

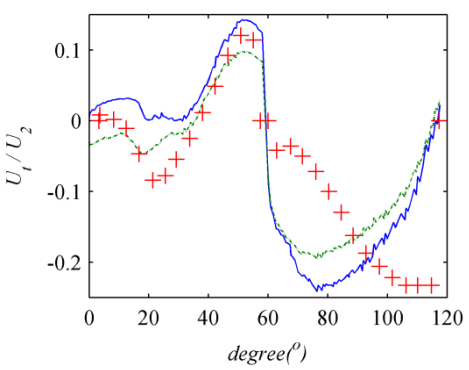

(b) tangential velocity at $0.5R_2$

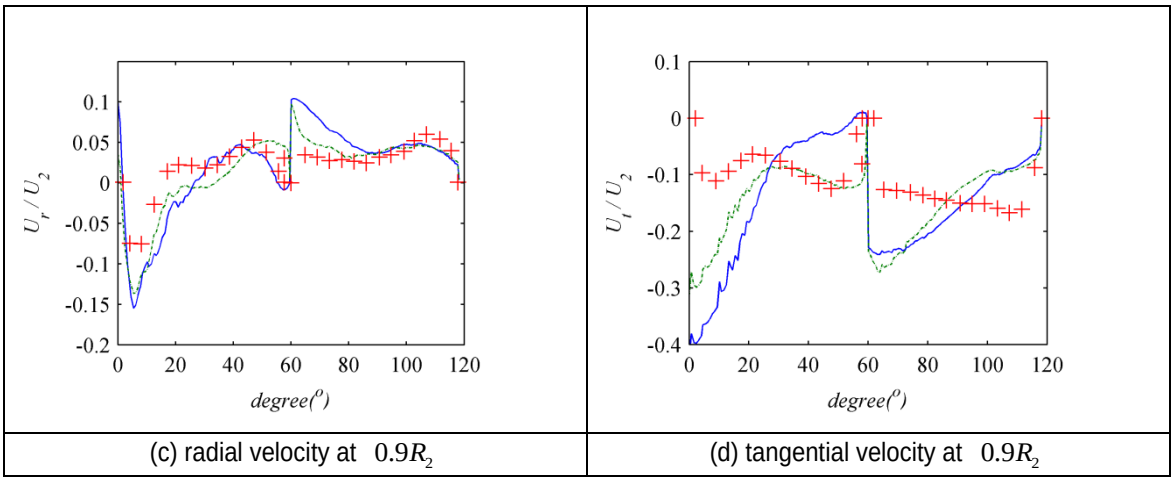

(c) radial velocity at $0.9R_2$ | (d) tangential velocity at $0.9R_2$

Figure 5. Comparison of Radial and tangential velocity profiles at part load(—:DSM, --:DNM, +:PIV results)

3. CONCLUSIONS

In this paper, the linear SGS model DSM and the non-linear model DNM are compared in the case of a centrifugal pump impeller at design load and quarter load. All the predicted time-averaged results are compared with the PIV experiments. At design load, the flow behaves well in both channels and the two models perform similarly. While at quarter load, the "two-channel" flow pattern occurs. Although this phenomenon is detected by both models, the peak value of the velocity profile moves towards the pressure side, showing opposite tendency to PIV. This is related to the prerotation ignored at inlet of the calculation, which is enough to affect the flow at channel B where the flow is well behaved, on the other hand, this effect is not sufficient to change the turbulent flow in channel A. Therefore, the calculated velocity profile agree well with PIV data in channel A. Comparing the two models under this condition, DNM shows significant priority over DSM due to the improved relation between the SGS stress, the shear-stress and vorticity. It can be concluded that non-linear model occupies much more potential at part-load condition. The flow field can be better reproduced by the non-linear model.

ACKNOWLEDGMENTS

The authors would like to acknowledge the financial supports given by the Ministry of Education, Science and Technology Project (Grant No. 113010A), the Research Fund for the Doctoral Program of Higher Education of China (Grant No. 20130008110047) and the National Natural Science Foundation of China (Grant No. 51209206).

REFERENCES

[1] J. Smagorinsky. General circulation experiments with the primitive equations: I. The basic euqations. *Mon. Weather*, 91:99-164, 1963.

[2] J.W. Deardorff. Three-dimensional numerical study of the height and mean structure of a heated planetary boundary layer. *Boundary-Layer Meteorology*. 7:81-106, 1974.

[3] B. Tao, J. Katz and C. Meneveau. Statistical geometry of subgrid-scale stresses determined from holographic particle image velocimetry measurements. *J. Fluid Mech.*. 457:35-78, 2002.

[4] K. Horiuti. Roles of non-aligned eigenvectors

of strain - rate and subgrid-scale stress tensors in turbulence generation. *J. Fluid Mech.*. 491:65-100, 2003.

[5] B. Kosovic. Subgrid - scale modelling for the large - eddy simulation of high-Reynolds - number boundary layers. *J. Fluid Mech.*. 336:151-182, 1997.

[6] B.C. Wang and D.J. Bergstrom. A dynamic nonlinear subgrid-scale stress model. *Physics of Fluids*. 17:035109 - 035109 - 15, 2005.

[7] M. Germano. Turbulence: the filtering approach. *J. Fluid Mech.*. 238:325-336, 1992.

[8] N. Pedersen, P.S. Larsen and C.B. Jacobsen. Flow in a centrifugal pump impeller at design and off-design conditions-Part I: particle image velocimetry (PIV) and laser Doppler velocimetry (LDV) measurements. *Journal of Fluids Engineering*. 125:61-72, 2003.

[9] OpenCFD. OpenFOAM®, The Open Source CFD Toolbox, *User Guide*, OpenCFD ltd, Berkshire, 2012

[10] D.K. Lily. A proposed modification of the Germano subgrid-scale closure method. *Phys. Fluids A*. 4:633-635, 1992.

[11] T.S. Lund, E.A. Novikov. Parametrization of subgrid-scale stress by the velocity gradient tensor. *Annual Research Briefs-Center for Turbulence Research*. 27 - 43, 1992.

[12] I.S. Celik, U. Ghia, P.J. Roache and C.J. Freitas. Procedure for estimation and reporting of uncertainty due to discretization in CFD applications. *Journal of Fluids Engineering*. 130:078001-1, 2008.

[13] P.J. Zhou. Investigation of stall characteristics in centrifugal pumps. China Agricultural University, Beijing, 2015.